Supporting information for: Macroscopic Salt Rejection through Electrostatically Gated Monolayer Porous Graphene

Roman M. Wyss,[†,§] Tian Tian,[‡,§] Khadija Yazda,[¶] Hyung Gyu Park,[¶] and Chih-Jen Shih[*,‡]

†*Institute of Soft Materials Department of Material Sciences, Eidgenössische Technische Hochschule (ETH) Zürich, Vladimir-Prelog-Weg 1-5, Zürich CH-8093, Switzerland.*

‡*Institute for Chemical and Bioengineering Department of Chemistry and Applied Biosciences, Eidgenössische Technische Hochschule (ETH) Zürich, Vladimir-Prelog-Weg 1-5, Zürich CH-8093, Switzerland.*

¶*Nanoscience for Energy Technology and Sustainability, Department of Mechanical and Process Engineering, Eidgenössische Technische Hochschule (ETH) Zürich, Tannenstrasse 3, Zürich CH-8092, Switzerland.*

§*R. M. S. and T. T. contributed equally to this work*

E-mail: chih-jen.shih@chem.ethz.ch

S1 Supplementary Section 1. Graphene membrane manufacturing and results.

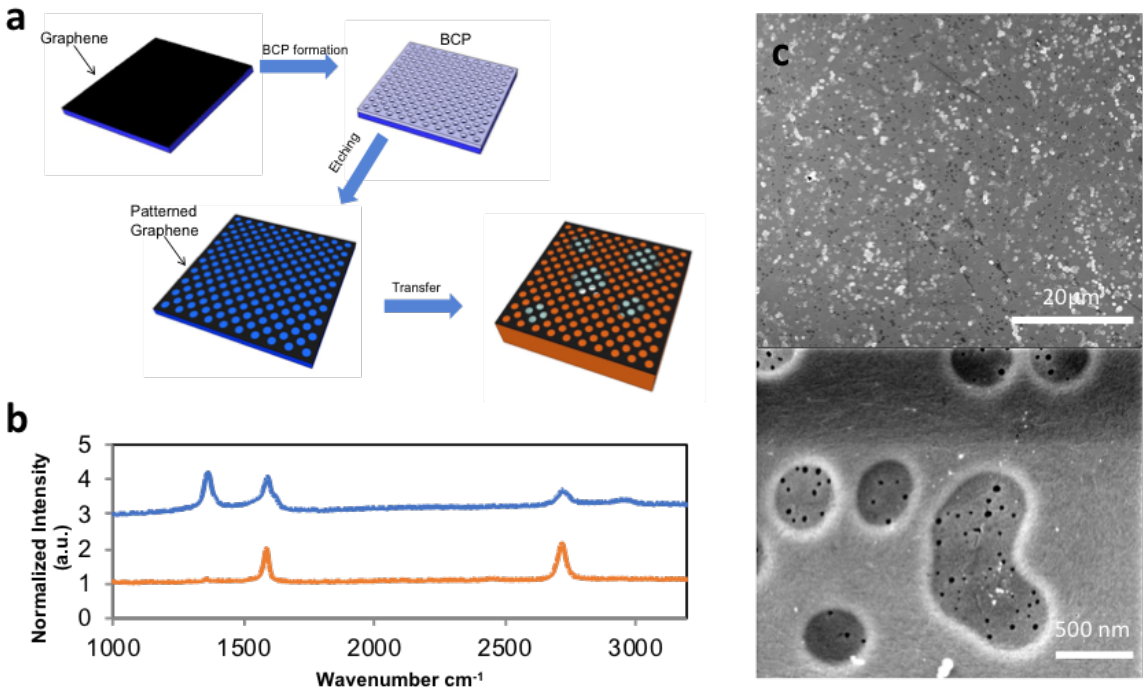

Figure S1: **a**. Schematic of manufacturing process for patterning of double layer graphene. Graphene is synthesized and transferred to a substrate (glass slide) to yield a double layer. BCP is spun and annealed in vacuum to undergo microphase separation, followed by plasma etch and wet etching yielding a porous polystyrene (PS) mask. Anisotropic etching of the mask leads to patterning the underlying graphene, PS is removed by thermal annealing. The porous graphene is then transferred to a substrate (e.g. PCTE). **b**. Raman spectra of graphene before (unpatterned, orange curve) and after (patterned, blue curve). An increase of the D-peak at 1350 cm^{-1} indicates the formation of defects and edges. The spectra have been normalized to the G-peak intensity and offset for better clarity. **c**. SEM graph of patterned graphene on PCTE at lower (top) and higher (bottom) magnifications. Note that tears in graphene appear bright white with a black center.

Table S1: Different diffusivities for the anions and cations of the salts used in this work

do you need any reference?

. The theoretical diffusion through PCTE can be calculated using Eq. 1 in the main text and the diffusivities of the respective anion and cation.

Salt	D (10^9 m^2·s^{-1})
K^+	1.95
Na^+	1.33
Li^+	1.03
SO_4^{2-}	1.06
Ca^{2+}	0.79
Mg^{2+}	0.7
$Fe(CN)_6^{3-}$	0.90
Cl^-	2.03

S2 Supplementary Section 2. Ion diffusion measurement and calculation

The ion diffusion through b-PCTE has been performed using a sample sandwiched between two layers of Aluminum tape where the edges have been sealed using water-resistant epoxy (ACS Marine Epoxy) to avoid interlayer leakage pathways.[S1] The sample was inserted in the fixture following the same wetting procedure described in the main text and was kept wet for the entire series of experiments.

The conductivity increases s (mS·cm^{-1}·d^{-1}) is converted into ion permeation rates $\boldsymbol{J}_{\mathrm{PCTE}}$ (mol·m^{-2}·s^{-1}) by use of a calibration factor c_{f}, the volume of LCR (V_{LCR}) , the area of the membrane A and the time t as:

$$\boldsymbol{J}_{\mathrm{PCTE}} = \frac{sV_{\mathrm{LCR}}}{c_{\mathrm{f}}At} \tag{1}$$

The calibration factors for all salts have been obtained by a linear fit of conductivity versus concentration for 4 solutions with concentrations from 10^{-4} M to 10^{-2} M and extracting the resulting slope. The rest of the factors are V_{LCR} = 7.33 mL, $A = 9\times10^{-6}$ m^{-2}. Table S2 shows the averaged conductivity increase s, the extracted calibration factors c_{f} and the resulting ion permeation rates using Eq. 1. The values from this table are shown in main text Fig.2b (blue bars).

Table S2: Extracted slope s as an averaged result from 3 consecutive measurements, the calibration factors c_f and the resulting ion permeation $\boldsymbol{J}_\mathrm{PCTE}$ through b-PCTE membranes for all salts.

Salt	s (mS·cm^{-1}d^{-1})	c_f (mS·cm^{-1}·mol^{-1}·ml)	$\boldsymbol{J}_\mathrm{PCTE}$ (10^6 mol·m^{-2}·s^{-1})
KCl	0.0151 ± 0.00265	106	1.34 ± 0.235
NaCl	0.0099 ± 0.000173	91	1.02 ± 0.0179
LiCl	0.00603 ± 0.000802	83	0.679 ± 0.0903
$CaCl_2$	0.0125 ± 0.001	149	0.789 ± 0.0631
$MgSO_4$	0.0088 ± 0.0012	130	0.633 ± 0.084
$K_3Fe(CN)_6$	0.024 ± 0.00275	395	0.575 ± 0.0633
K_2SO4_4	0.0198 ± 0.00199	258	0.722 ± 0.0726

S3 Control experiment with copper tape

We make sure that the applied voltage is effectively applied via the graphene membrane and not through leakage directly coupling the coppertape to the ionic solution. For this, we use a device as in Fig.1c

which figure?

, omitting the graphene and measuring the current through the membrane with the Autolab electrochemical workstation using the membrane as working electrode and a platinum wire as counter/reference electrode 3.5 cm apart in 0.1 mM KCl. When no graphene is inserted in the device, a current in the baseline range ($\sim$ 0.1 nA) is observed, indicating no current passing from the membrane. However, if graphene is inserted, a current in the range of $\sim$ 10 - 100 nA is measured. If the copper tape is in contact with the solution when omitting the Kapton tape, the current increases to $\sim$ 1 - 10 μA, independent of the exposed area of the copper tape to the solution.

S4 KCl Debye length and conductivity

Table S3 gives an overview about the measured conductivities and their calculated Debye lengths for KCl. The information is used to plot the rectification versus concentration.

Table S3: Conductivity and calculated Debye lengths of various KCl concentrations in order to obtain rectification versus concentration curves.

c_0 (mM)	Conductivity (mS·cm^{-1})	λ_{D} (nm)
0.1	0.01903	30.4
0.33	0.0541	16
1	0.1329	10
3.3KCl	0.513	6
10KCl	1.08	3.3

S5 Further details of the numerical simulation

The numerical simulations were carried out using COMSOL Multiphysics 5.3a. The simulation domain is shown in Fig.S2. To simplify the geometry, we use axial symmetric coordinate system. The radius *L* and height *H* of both HCR and LCR are set to 20 R_{G}, the radius of the nanopore. The potential at the bottom of the LCR and the center of the graphene domains are set to be 0 and ψ_{G}, respectively. The potential at the end of HCR is not set explicitly, but rather determined through the Poisson equation with no flux boundary condition $\boldsymbol{D}^{\mathrm{norm}} = 0$. The relative permittivity in the HCR and LCR is set as $\varepsilon = 78$. The relative permittivity of the Stern layer is set to $\varepsilon_{\mathrm{H}} = 20$[S2] and for the graphene domain we set the relative permittivity as a large number (e.g. 10^5) for a better convergence of the solver. For the transport of diluted ionic species, we use the PNP equations to describe the diffusion and drift of the ions, which can be further unified by the gradient of electrochemical potential, as described in the main text. The initial values of the electrolyte is set to c_0 in HCR and 0.1 c_0 in LCR. At the ends of the cells in the z-direction, we use the inlet boundaries conditions for the concentration of electrolytes, that the concentration on these boundaries remains the same with the initial value, due to the effective mixing in the experimental setup.

The transport of ionic species is described by the steady-state Nernst-Planck equation:

$$\nabla \cdot \boldsymbol{J}_i = -\nabla \cdot \left(\frac{D_i}{k_{\mathrm{B}}T} c_i N_{\mathrm{A}} \nabla \mu_i \right) = -\nabla \cdot \left(\frac{D_i}{k_{\mathrm{B}}T} c_i N_{\mathrm{A}} [k_{\mathrm{B}}T \nabla \ln x_i + z_i e \nabla \psi] \right) = 0 \tag{2}$$

$$x_i = \frac{c_i}{\sum_i c_i + c_{\mathrm{H_2O}}} \tag{3}$$

The potential distribution within the whole simulation domain is described by the Poisson equation:

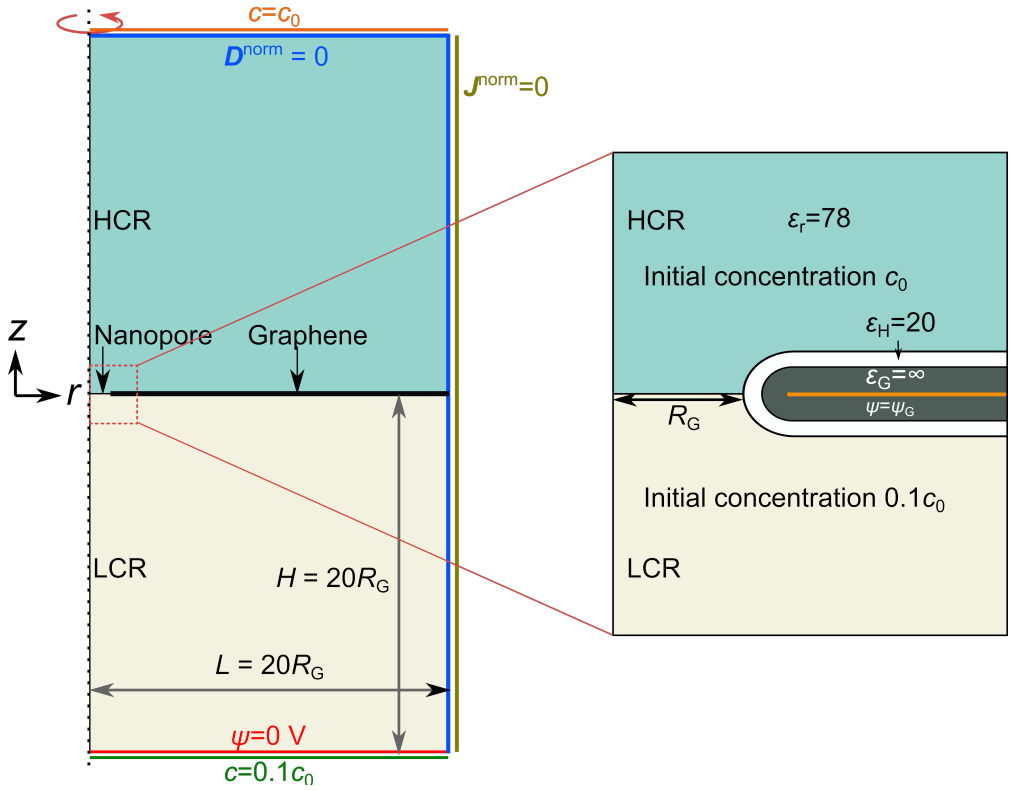

Figure S2: Scheme of the simulation domain used. Left: geometry of the whole simulation domain. Right: configuration near the graphene nanopore, corresponding to the red rectangle on the left side.

$$\nabla \cdot (\varepsilon_{\mathrm{m}} \varepsilon_0 \nabla \psi) = -N_{\mathrm{A}} e \sum_i c_i z_i \tag{4}$$

Where ε_{m} is the relative permittivity of domain m. The contribution of mobile charges is only valid in the solution domain. The use of a large ε_{G} ensures that the potential in the whole simulation domain can be solved continuously.

To simulate the applied external bias V_{G}, we set the value of ψ_{G} explicitly and extract the charge σ_{G} by:

$$\sigma_{\mathrm{G}} = -\frac{\int_\Omega z_i c_i N_{\mathrm{A}} e \mathrm{d}^3\Omega}{S_{\mathrm{G}}} \tag{5}$$

and V_{G} is then calculated by:

$$V_{\mathrm{G}} = \Delta\phi_{\mathrm{G}} + \psi_{\mathrm{G}} \tag{6}$$

$$\sigma_{\mathrm{G}} = \int_0^{\Delta\phi_{\mathrm{G}}} \frac{1}{C_{\mathrm{Q}}(\phi_{\mathrm{G}})} \mathrm{d}\phi_{\mathrm{G}} \tag{7}$$

where the quantum capacitance $C_{\mathrm{Q}} = \partial\sigma_{\mathrm{G}}/\partial\phi_{\mathrm{G}}$ is calculated by Eq. 8 in main text.

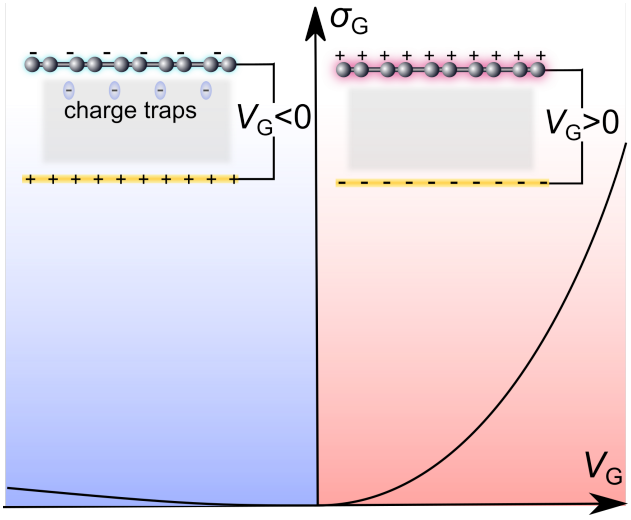

Figure S3: Schematic illustration of the origin of the asymmetric rectification with respect to V_{G}. Due to the existence of surface charge traps at negative V_{G}, the graphene is less charged compared to the positive V_{G}.

Note that due to the existence of electron traps on graphene due to fabrication process, the

induced charge traps on graphene effectively reduce the charge density on graphene and greatly attenuate the surface potential on graphene, as illustrated in Fig.. S3. This effect is universally observed in CVD-graphene-based field effect transistors in air, while the mechanism is fully understood yet. In view of this, we only simulate the situation where $V_{\mathrm{G}} > 0$ for the salt rejection mechanism. The trend that ξ is almost independent of V_{G} when $V_{\mathrm{G}} < 0$ can be qualitatively explained by the existence of surface charge traps as stated above.

S6 Further numerical simulation results

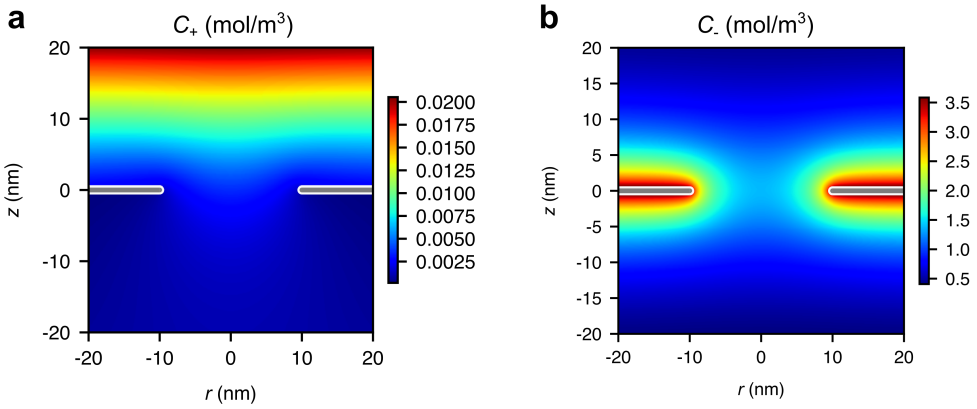

Figure S4: Cation concentration c_+ (**a**.) and anion concentration c_- (**b**.) near the graphene nanopore for KCl solution at 0.1 mM. Depletion of cation and accumulation of anion can be observed near the graphene surface.

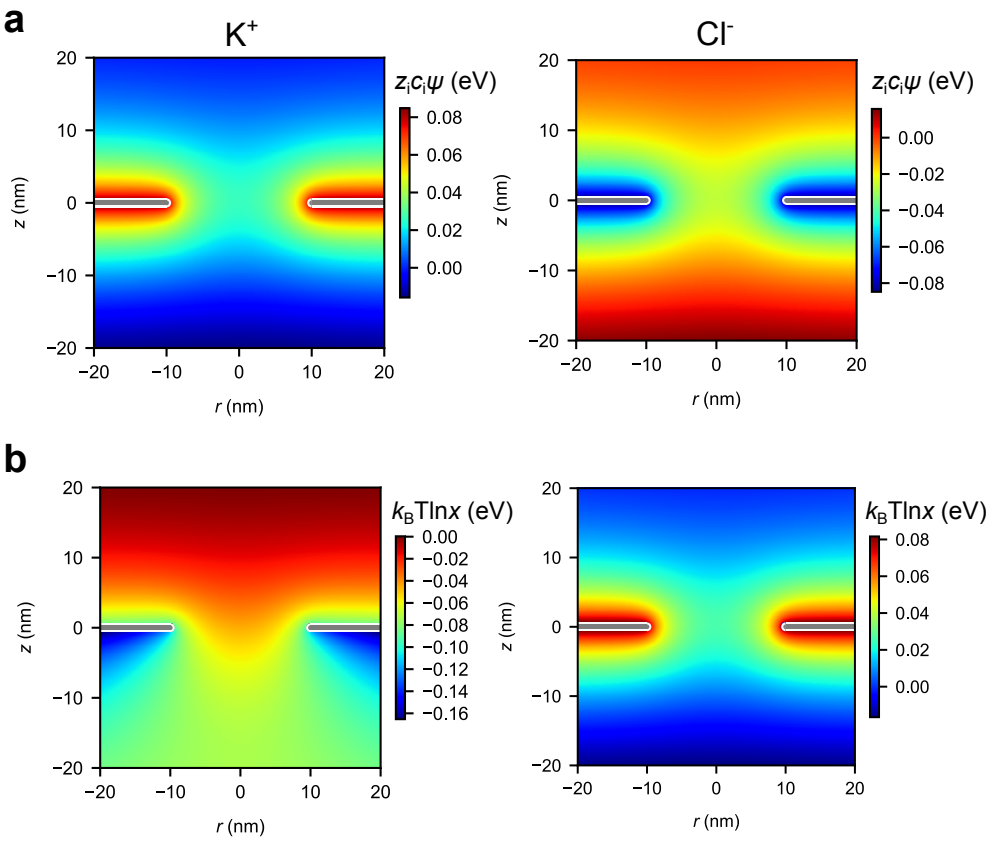

Figure S5: Decomposition of electrochemical potential near a nanopore corresponding to Fig.4 in main text. **a**. The electrostatic (drift) contribution to the electrochemical potential for cation (left) and anion (right) and **b**. The concentration (diffusion) contribution to the electrochemical potential for cation (left) and anion (right). The relative small order of magnitude for anion electrochemical potential is caused by the balance between the diffusion and drift for anion.

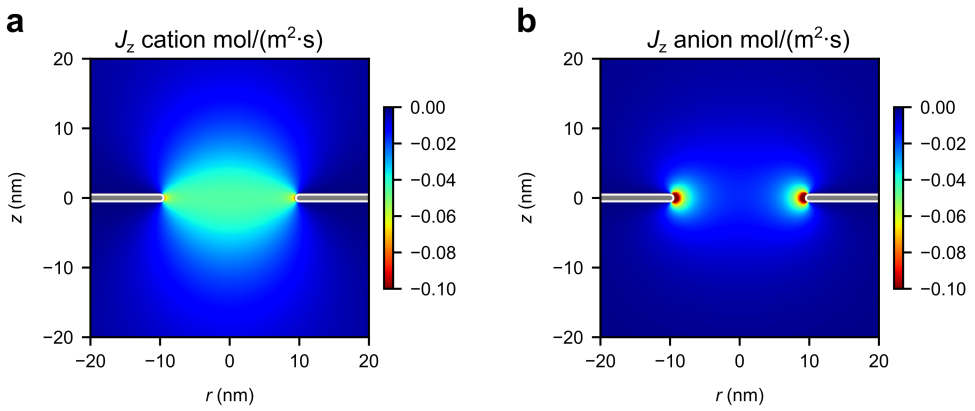

Figure S6: z-component flux $\boldsymbol{J}_z$ of cation (**a**.) and anion (**b**.) near the graphene nanopore corresponding to Figure 4b in main text. The pathways for the different ions can be spatially distinguished: the flux of cation passes mostly through the center of the graphene nanopore while the anion passes mainly through the edge. The analysis is in consistent with the gradient of chemical potential as shown in the main text Fig.4b.

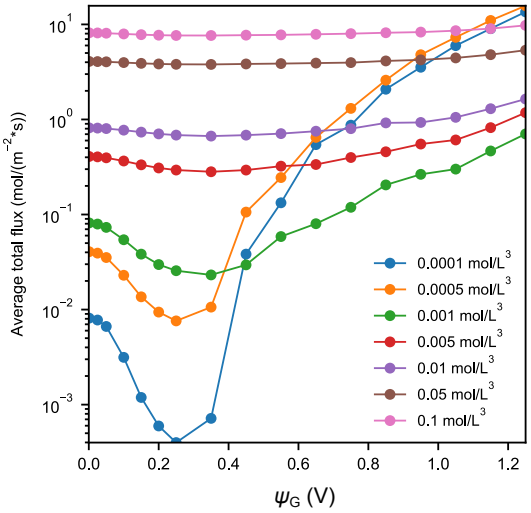

Figure S7: Average total flux $\boldsymbol{J}_z$ in the nanopore as a function of ψ_{G} at different concentrations. The range of ψ_{G} is larger than the experimentally achievable value. The rectification of flux becomes weaker after a certain level of ψ_{G} is reached. Further increasing the surface potential of graphene may even enhance the transportation of ions, which is similar to the cases of ionic transistors.

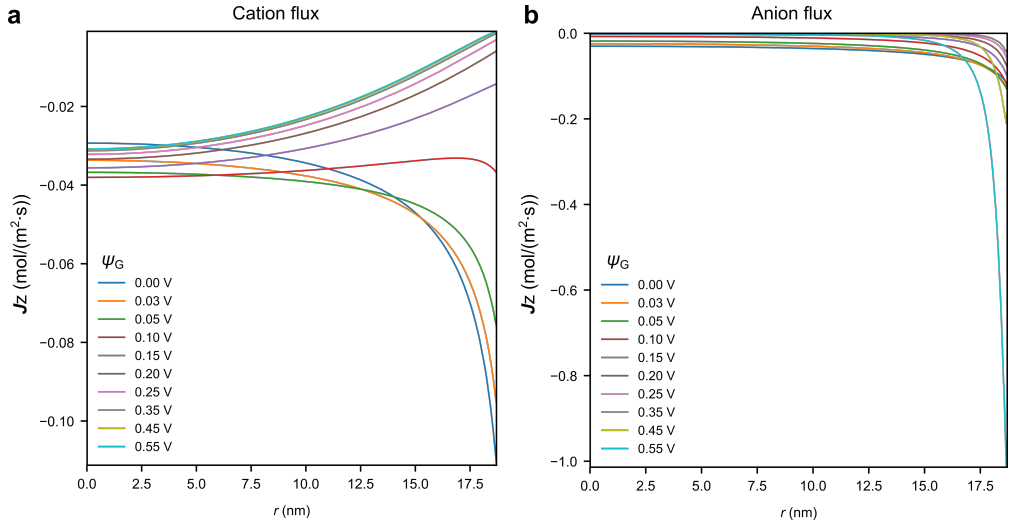

Figure S8: Spatial distribution of $\boldsymbol{J}_z$ as a function of r in a 20 nm nanopore at different levels of ψ_{G} (larger than experimentally achievable values) for cation (**a**.) and anion (**b**.). The cation flux becomes nearly saturated with increasing ψ_{G}, while the flow of anion near the pore edge becomes much larger. The drastic increase of pore-bounded anion flux is caused by the accumulation of anions near the graphene surface, and in turn causes the increasing of total flux as seen in Fig.S7.

S7 Conductivities and Debye length for all salts

In Table S3, the conductivities and calculated Debye lengths for 6 salts are shown. At the same concentration, the higher ionic strength of the multivalent salts leads to a reduction of the respective Debye lengths.

Table S4: conductivity

Solution	Conductivity ($mS \cdot cm^{-1}$)	λ_D (nm)
0.1 mM NaCl	0.018	30.4
0.1 mM LiCl	0.0158	30.4
0.1 mM $CaCl_2$	0.02187	17.2
0.1 mM $MgSO_4$	0.0327	15.2
0.1 mM K_2SO_4	0.0416	17.2
0.1 mM $K_3(Fe(CN)_6)$	0.0595	9.6

References

(S1) Choi, K.; Droudian, A.; Wyss, R. M.; Karl-Philipp, S.; Park, H. G. *Sci. Adv.* **2018**, *in press*.

(S2) Conway, B. E.; Bockris, J. O.; Ammar, I. A. *Trans. Faraday Soc.* **1951**, *47*, 756–766.